15. See supporting material on *Science* Online.
16. L. B. Haberly, *Chem. Senses* **26**, 551 (2001).
17. D. J. Calu, M. R. Roesch, T. A. Stalnaker, G. Schoenbaum, *Cereb. Cortex* **17**, 1342 (2007).
18. E. Pastalkova *et al.*, *Science* **313**, 1141 (2006).
19. R. Shema, T. C. Sacktor, Y. Dudai, *Science* **317**, 951 (2007).
20. B. Sacchetti, T. Sacco, P. Strata, *Eur. J. Neurosci.* **25**, 2875 (2007).
21. J. Coleman, W. J. Clerici, *Brain Res.* **194**, 205 (1980).
22. C. Shi, M. Davis, *J. Neurosci.* **21**, 9844 (2001).
23. D. S. Barth, N. Goldberg, B. Brett, S. Di, *Brain Res.* **678**, 177 (1995).
24. X. O. Zhu, M. W. Brown, B. J. McCabe, J. P. Aggleton, *Neuroscience* **69**, 821 (1995).
25. P. W. Frankland, B. Bontempi, L. E. Talton, L. Kaczmarek, A. J. Silva, *Science* **304**, 881 (2004).
26. T. Maviel, T. P. Durkin, F. Menzaghi, B. Bontempi, *Science* **305**, 96 (2004).
27. B. Sacchetti, C. A. Lorenzini, E. Baldi, G. Tassoni, C. Bucherelli, *J. Neurosci.* **19**, 9570 (1999).
28. G. D. Gale *et al.*, *J. Neurosci.* **24**, 3810 (2004).
29. Y. Lee, D. Walker, M. Davis, *Behav. Neurosci.* **110**, 836 (1996).
30. B. Sacchetti, E. Baldi, C. A. Lorenzini, C. Bucherelli, *Proc. Natl. Acad. Sci. U.S.A.* **99**, 8406 (2002).
31. B. Sacchetti, B. Scelfo, F. Tempia, P. Strata, *Neuron* **42**, 973 (2004).
32. E. L. Malin, J. L. McGaugh, *Proc. Natl. Acad. Sci. U.S.A.* **103**, 1959 (2006).
33. F. Gonzalez-Lima, T. Finkenstädt, J. P. Ewert, *Brain Res.* **489**, 67 (1989).
34. A. Poremba, D. Jones, F. Gonzalez-Lima, *Eur. J. Neurosci.* **10**, 3035 (1998).
35. D. A. Wilson, C. Linster, *J. Neurophysiol.* **100**, 2 (2008).
36. H. Wan *et al.*, *Eur. J. Neurosci.* **14**, 118 (2001).
37. D. M. Diamond, N. M. Weinberger, *Behav. Neurosci.* **98**, 189 (1984).
38. A. E. Villa, I. V. Tetko, B. Hyland, A. Najem, *Proc. Natl. Acad. Sci. U.S.A.* **96**, 1106 (1999).
39. W. Li, J. D. Howard, T. B. Parrish, J. A. Gottfried, *Science* **319**, 1842 (2008).
40. G. Paxinos, C. Watson, *The Rat Brain in Stereotaxic Coordinates* (Academic Press, New York, 1986).
41. We thank J. L. McGaugh for critical comments on the manuscript and L. Milano, A. Renna, D. Germano, V. Pastrone, D. Tonello, and G. Benvenuti for technical assistance. Supported by grants from the Italian Ministry of University.

Supporting Online Material

www.sciencemag.org/cgi/content/full/329/5992/649/DC1
Materials and Methods
SOM Text
Figs. S1 to S10
References

12 October 2009; accepted 18 June 2010
10.1126/science.1183165

REPORTS

Normal Modes and Density of States of Disordered Colloidal Solids

D. Kaya,[1] N. L. Green,[2] C. E. Maloney,[3] M. F. Islam[1,2]*

The normal modes and the density of states (DOS) of any material provide a basis for understanding its thermal and mechanical transport properties. In perfect crystals, normal modes are plane waves, but they can be complex in disordered systems. We have experimentally measured normal modes and the DOS in a disordered colloidal crystal. The DOS shows Debye-like behavior at low energies and an excess of modes, or Boson peak, at higher energies. The normal modes take the form of plane waves hybridized with localized short wavelength features in the Debye regime but lose both longitudinal and transverse plane-wave character at a common energy near the Boson peak.

Normal modes provide a framework for understanding the dynamical excitations of a system in diverse fields ranging from architecture to molecular biology. The normal modes are those degrees of freedom which, at least for small perturbations away from equilibrium, do not interact with each other. Each mode oscillates independently of the others with its own characteristic frequency. The distribution of these frequencies, known as the density of states (DOS), and the structure of the modes are used as a starting point to calculate the heat capacity, thermal conductivity, and elastic constants in solids (*1*).

In a perfect crystal, due to the translational symmetry, the normal modes must be plane waves. Once disorder is introduced into a perfect crystal, the modes become more complicated, and the related DOS and thermodynamical properties begin to deviate from those in the perfect system. The disorder can be geometrical in nature, as in the case of structural glasses (*2*). Even geometrically perfect crystals can become disordered if the interactions between nearest neighbors or the masses of the particles are not uniform (*3*). In fact, disordered crystals are often used as a simple theoretical framework to understand generic emergent behavior in other types of disordered systems, such as structural glasses (*4*–*6*). In theoretical models of both disordered crystals and structural glasses, the key features that emerge are a Debye-like regime with hybridization of localized regions of low shear modulus with the low-frequency (long wavelength) plane waves, and an excess in the DOS at higher frequencies known as the Boson peak (*4*, *5*, *7*–*9*). Normal modes and the DOS have not been directly measured experimentally in a disordered system, in part because for the case of disordered atomic systems, directly tracking the dynamics of individual atoms is not experimentally feasible.

Colloidal suspensions have been used as model systems to study various phenomena that occur in other condensed matter systems, such as atomic liquids, crystals, and glasses (*10*–*15*). In colloidal systems, one may use optical microscopy to observe individual particle motions within the interior of a system (*10*, *14*, *13*). With traditional hard-sphere colloidal particles such as silica spheres, one may readily produce a crystal or an amorphous structural glass. However, the perfect crystals produced with these conventional particles show spatially homogeneous fluctuations (*16*–*20*). Here, we studied a face-centered-cubic (fcc) crystal made of deformable microgel colloidal particles with essentially perfect geometrical order yet strongly heterogeneous fluctuations. The heterogeneity may be caused by particle-to-particle variations in the microgel stiffness and is a novel characteristic of the deformable microgel colloids (*15*).

Normal mode energies of perfect colloidal crystals are usually obtained by assuming a plane-wave form for the modes and then measuring the amplitudes of the plane waves (*16*, *17*, *20*), much as

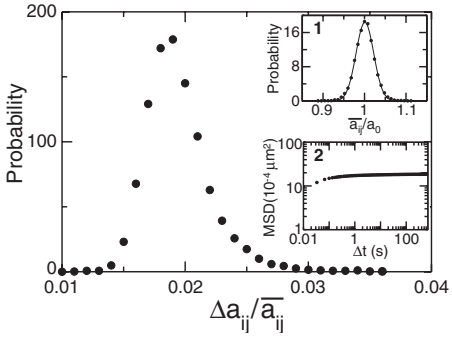

Fig. 1. Probability distribution of temporal fluctuations in nearest-neighbor spacing $\Delta a_{ij}/\overline{a}_{ij}$. The distribution is quite wide, with an average of about 1.9% and an RMS width of about 0.23%. (**Inset 1**) Probability distribution of nearest-neighbor spacing in the equilibrium configuration, $\overline{a}_{ij}/a_0$. The relative spatial fluctuations in $\overline{a}_{ij}$ were about 2.1%. The solid line is a Gaussian fit through the data. The spatial fluctuations in Δa_{ij} were ~5 times as large as the spatial fluctuations in $\overline{a}_{ij}$. (**Inset 2**) MSD averaged over particles reaches a well-defined plateau.

[1]Department of Materials Science and Engineering, Carnegie Mellon University, 5000 Forbes Avenue, Pittsburgh, PA 15213–3890, USA. [2]Department of Chemical Engineering, Carnegie Mellon University, 5000 Forbes Avenue, Pittsburgh, PA 15213–3890, USA. [3]Department of Civil and Environmental Engineering, Carnegie Mellon University, 5000 Forbes Avenue, Pittsburgh, PA 15213–3890, USA.

*To whom correspondence should be addressed. E-mail: mohammad@cmu.edu

one obtains the dispersion curves in an atomic system through scattering experiments (*1*). However, for any disordered system with heterogeneity, such as our system, one cannot assume, a priori, that the normal modes are plane waves. Therefore, we developed an approach to measure the correlations in particle displacements to determine the normal modes themselves and their DOS (*21*). The anomalous normal mode structure and DOS of our microgel colloidal system exhibited some theoretically predicted universal features of both disordered crystals (*4*, *5*) and structural glasses (*7*–*9*) and provided insights into the origin of the Boson peak. Moreover, our approach is quite general and can also be used to directly reconstruct the normal modes of other colloidal systems such as structural glasses, perfect crystals with isolated point or line defects, and the like.

The degree of geometrical order of the equilibrium configuration and the spatial heterogeneity of the fluctuations away from equilibrium in our system are shown in Fig. 1. Time-averaged positions, $\overline{\vec{r}_i}$, of the particles were computed from the tracks, and particle displacements were calculated as $\vec{u}_i(t) = \vec{r}_i(t) - \overline{\vec{r}_i}$. The resolution in particle displacements was less than 5 nm (*22*, *23*). Single-particle displacement distributions were Gaussian, with an anisotropy of less than 0.07. The nearest-neighbor separations, $\overline{a}_{ij} = |\overline{\vec{r}_i} - \overline{\vec{r}_j}|$, between the time-averaged positions of the centers of all particles were more or less homogeneous throughout the system (fig. S2). The spatial average value of $\overline{a}_{ij}$, denoted as a_0, was 1.18 μm. The normalized probability distribution of $\overline{a}_{ij}/a_0$, shown in inset 1 of Fig. 1, had a relative root mean square (RMS) variation of 2.1%. This demonstrates the relatively high degree of geometrical order in our system. The average mean squared displacement (MSD) with a clear plateau indicating solid-like behavior and the absence of diffusion are shown in inset 2 of Fig. 1.

We then focused on the temporal fluctuations in the instantaneous nearest-neighbor separations, $a_{ij}(t) = |\vec{r}_i(t) - \vec{r}_j(t)|$, to determine the degree of disorder in our system. The time-dependent fluctuations of $a_{ij}(t)$ for four random pairs of particles are shown in fig. S3. Because the fluctuations in $a_{ij}(t)$ (fig. S3) and the average RMS particle displacements (inset 2 of Fig. 1) were significantly larger than the experimental resolution in particle displacements, our subsequent analyses are not limited by experimental resolution (*24*). The temporal RMS fluctuations for each pair, $\Delta a_{ij} = \sqrt{\overline{(a_{ij}(t) - \overline{a}_{ij})^2}}$, are shown in fig. S4, and the probability distribution of the normalized values, $P(\Delta a_{ij}/\overline{a}_{ij})$, is shown in the main plot of Fig. 1. Without heterogeneous interactions between the particles, in a geometrically ordered colloidal crystal like ours, the Δa_{ij} would necessarily be identical and $P(\Delta a_{ij}/\overline{a}_{ij})$ would be very narrow. It is the internal degrees of freedom corresponding to the stiffness of individual hydrogel particles that can allow for these particle-to-particle variations in our system. The values of Δa_{ij} for any given pair defined over intermediate time windows were relatively steady over the entire duration of data collection and did not depend on time-averaging. The average $\Delta a_{ij}/\overline{a}_{ij}$ was about 1.9%, and the width of the distribution was 0.23%, which shows that the spatial fluctuations in Δa_{ij} were approximately five times as large as the spatial fluctuations in a_{ij}. We verified that there was virtually no correlation between Δa_{ij} and $\overline{a}_{ij}$ for any given pair (i.e., there was little correlation between figs. S2 and S4), indicating that the heterogeneous dynamics was due to nonuniform interactions between particles rather than geometrical irregularities in the crystal. The local MSDs of individual particles were also spatially heterogeneous, giving further indication of the presence of nonuniform interactions. We have performed molecular dynamics simulations with crystals of soft particles of spatially uncorrelated stiffness that showed regions of correlated dynamical fluctuations (fig. S5) similar to the ones observed here (fig. S4), despite the underlying uncorrelated particle stiffness (*21*).

Next, we determined the normal modes from the observed particle displacement fields (*25*). In a harmonic system governed by equipartition of energy, the two-point correlations, $G_{i\alpha j\beta} \doteq \langle u_{i\alpha} u_{i\beta} \rangle$ (where the Latin letters index particles and the Greek letters index Cartesian components with an implicit Einstein summation convention), are given in terms of the normal modes as (*26*): $G_{i\alpha j\beta} = \sum_p (\psi^p_{i\alpha} \psi^p_{j\beta}) k_B T/\lambda_p$, where $\psi^p_{i\alpha}$ is the p-th normal mode, λ_p is the p-th energy eigenvalue, k_B is the Boltzmann constant, and T is the temperature. That is, the normal modes are those degrees of freedom that appear uncorrelated with a mean squared amplitude of $k_B T/\lambda_p$. We emphasize that no assumptions are made about the underlying dynamics beyond that they give the appropriate probability for observing a given fluctuation away from the equilibrium configuration. If one knows the structure of the $\psi^p_{i\alpha}$ a priori, for example in a homogeneous perfect crystal where the $\psi^p_{i\alpha}$ must be plane waves, one may decompose $u_{i\alpha}$ onto the known

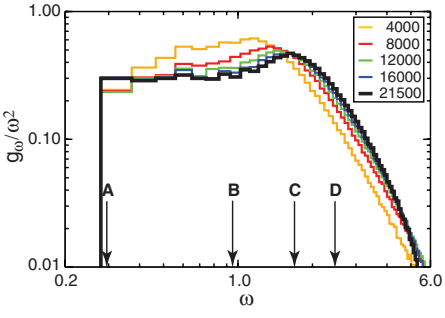

Fig. 2. g_ω, divided by ω^2. The different colored curves correspond to different statistical ensemble size, that is, the total number of statistically independent images used to compute the sample covariance. The DOS shows Debye-like behavior, constant g_ω/ω^2, at low energy with a Boson peak at higher energy. Points A to D correspond to the ω values of four modes shown in detail in Fig. 3.

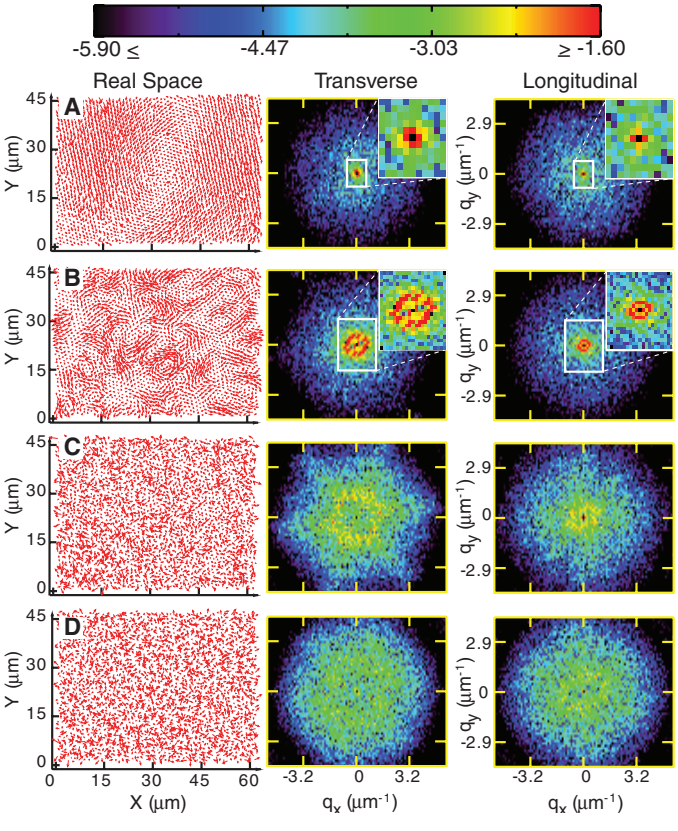

Fig. 3. (**A** to **D**) Four normal modes taken from various regimes indicated in Fig. 2. For each mode, we show the normalized mode vectors in real space along with the squared amplitude of the projection onto transverse and longitudinal plane waves. In the Debye regime, the intensity is peaked in Fourier space around a characteristic wavevector, q_0. Above the Boson peak, the intensity distribution is uniform throughout the Brillouin zone.

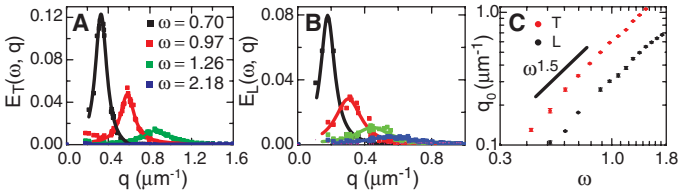

Fig. 4. The ω and *q*-averaged Fourier decompositions of the normal modes along (**A**) the transverse (T) and (**B**) the longitudinal (L) plane waves versus *q* for a few ω values. The solid lines are Lorentzian fits through the data. (**C**) q_0, obtained from the Lorentzian peak location, plotted against ω shows that $q_0 \sim \omega^{3/2}$.

$\psi^p_{i\alpha}$ and use these mode amplitudes to estimate (*17*) $\lambda_p/k_BT = \langle(\sum_i u_{i\alpha}\psi^p_{i\alpha})^2\rangle^{-1}$.

When one does not know the $\psi^p_{i\alpha}$ a priori, such as for disordered systems like ours, other methods are necessary to estimate the λ_p and the ψ_{ip} themselves. To do this, one may diagonalize the observed two-point correlations, $\hat{G}_{ij}$, the so-called sample covariance, to obtain the ψ_{ip}. This procedure has been used to infer normal modes in simulations of small molecular systems (*27*), but care must be taken when applying it to larger systems. It is known that the procedure is highly sensitive to the number of independent observations (*28*). However, we have observed that the spectrum of energy eigenvalues converged by about 20,000 independent observations of the displacement field.

In conventional studies of disordered systems, one generally normalizes the observed DOS by the Debye prediction (*4*, *5*, *7*–*9*), where a plateau is obtained at low energy. Because we observed a two-dimensional (2D) slice of a 3D system, we first determined the appropriate normalization factor for our observed DOS. At low ω, where $\omega = \sqrt{\mathrm{MSD}\lambda/(k_BT)}$, the DOS, $g_\omega = dN/d\omega$, exhibited a power-law regime for almost a decade where $dN/d\omega \sim \omega^2$ and *N* is the index of the mode. We therefore normalized g_ω by ω^2. Here, we introduce ω to make connections with theoretical work where one usually works with $\sqrt{\lambda}$ rather than λ.

In Fig. 2, we show g_ω/ω^2. Each histogram corresponds to a sample covariance obtained using a different total number of independent displacement field observations: 4000, 8000, 12,000, 16,000, and 21,500, indicating that the spectrum has converged. Below $\omega \approx 1.2$, g_ω/ω^2 shows a Debye-like plateau. At higher ω, g_ω/ω^2 rises to a Boson peak at $\omega \sim 1.7$ before rapidly falling. This general behavior is consistent with that seen generically in numerical models of structural glasses (*29*, *7*, *8*, *30*, *31*, *9*) and elastically disordered lattices (*5*, *4*).

To analyze the spatial structure of the modes, we decomposed them onto longitudinal and transverse plane waves using standard Fourier analysis techniques. Figure 3 shows four modes taken from various regions of the spectrum, as indicated in Fig. 2. In the Debye regime, the modes, shown in Fig. 3, A and B, were composed primarily of plane waves with a single dominant wavevector, q_0, which were hybridized with localized short-wavelength features. On approach to the Boson peak, q_0 saturated at q_{BP}, which corresponds to about five to six particle diameters for the transverse plane waves and about twice that wavelength for the longitudinal plane waves. Above the Boson peak, the intensity was distributed broadly throughout the Brillouin zone, and all plane-wave character was lost (Fig. 3, C and D, and movie S1). Near the Boson peak, the effects of the lattice became noticeable, and the mode shown in Fig. 3C had pronounced broken symmetry with intensity accumulating around the six-fold symmetric crystal axes.

Our observation of the $g_\omega \sim \omega^2$ scaling of the DOS at low ω implies a relationship between q_0 and ω. Simply counting the number of plane waves in 2D gives $dN/dq \sim q$ (*1*). Then $d\omega/dq \sim (d\omega/dN)(dN/dq) \sim \omega^{-2}q$, which gives $q_0 \sim \omega^{3/2}$. To test this prediction and to quantitatively determine q_0 near q_{BP}, we determined q_0 as a function of ω. We first averaged the Fourier decompositions along transverse and longitudinal plane waves over a small range (~10%) of ω. Then the ω-averaged Fourier decompositions were averaged over angles (again, ~10% in *q*) to obtain $E_T(\omega, q)$ and $E_L(\omega, q)$, where subscripts *T* and *L* were contributions along the directions of transverse and longitudinal plane waves. For each ω, we found that, below the Boson peak, $E_T(\omega, q)$ and $E_L(\omega, q)$ could be fit to a Lorentzian profile. Several of these $E_T(\omega, q)$ and $E_L(\omega, q)$ with the Lorentzian fits (solid lines) at various ω are shown in Fig. 4, A and B. The location of the Lorentzian peak then gave q_0 for a given ω. Our analysis showed that $q_0 \sim \omega^{3/2}$, as shown in Fig. 4C. We also found that the point at which a Lorentzian fit became unfeasible was at an ω near the Boson peak, and this was true for both the longitudinal and transverse contributions.

In numerical models of structural glasses (*9*), only the transverse plane waves become overdamped near the Boson peak, and there was little correlation with the longitudinal modes. In contrast, in our system of disordered crystals, the sharply peaked contribution to the normal modes goes away for both longitudinal and transverse plane waves at the Boson peak. This raises the question of how the emergent properties of various kinds of disordered solids depend on the nature of the disorder.

In conclusion, we have determined the normal modes and DOS of a strongly disordered colloidal crystal composed of deformable microgel particles. This type of disorder is similar to that used in theoretical models. We have established that Debye-like behavior at low energy with a Boson peak at higher energy are generic features of disordered solids, whereas the nature of the vanishing of the plane-wave character near the Boson peak may depend on particular details of the disorder. The general procedure presented here will be an important tool to identify the impacts, at a particle-scale level, of different types of disorder on the structure of the normal modes and elasticity that are present in various atomic, molecular, and colloidal crystals and glasses.

References and Notes

1. N. W. Ashcroft, N. D. Mermin, *Solid State Physics* (Saunders College, Philadelphia, 1976).
2. S. R. Elliott, *Physics of Amorphous Materials* (Longmans, New York, 1990).
3. R. J. Elliott, J. A. Krumhansl, P. L. Leath, *Rev. Mod. Phys.* **46**, 465 (1974).
4. S. N. Taraskin, Y. L. Loh, G. Natarajan, S. R. Elliott, *Phys. Rev. Lett.* **86**, 1255 (2001).
5. W. Schirmacher, G. Diezemann, C. Ganter, *Phys. Rev. Lett.* **81**, 136 (1998).
6. A. Souslov, A. J. Liu, T. C. Lubensky, *Phys. Rev. Lett.* **103**, 205503 (2009).
7. H. R. Schober, *J. Phys. Condens. Matter* **16**, S2659 (2004).
8. H. R. Schober, C. Oligschleger, *Phys. Rev. B* **53**, 11469 (1996).
9. H. Shintani, H. Tanaka, *Nat. Mater.* **7**, 870 (2008).
10. W. K. Kegel, A. van Blaaderen, *Science* **287**, 290 (2000).
11. D. G. A. L. Aarts, M. Schmidt, H. N. W. Lekkerkerker, *Science* **304**, 847 (2004).
12. U. Gasser, E. R. Weeks, A. Schofield, P. N. Pusey, D. A. Weitz, *Science* **292**, 258 (2001).
13. A. M. Alsayed, M. F. Islam, J. Zhang, P. J. Collings, A. G. Yodh, *Science* **309**, 1207 (2005).
14. E. R. Weeks, J. C. Crocker, A. C. Levitt, A. Schofield, D. A. Weitz, *Science* **287**, 627 (2000).
15. J. Mattsson *et al.*, *Nature* **462**, 83 (2009).
16. Z. Cheng, J. Zhu, W. B. Russel, P. M. Chaikin, *Phys. Rev. Lett.* **85**, 1460 (2000).
17. P. Keim, G. Maret, U. Herz, H. H. von Grünberg, *Phys. Rev. Lett.* **92**, 215504 (2004).
18. H. H. von Grünberg, P. Keim, K. Zahn, G. Maret, *Phys. Rev. Lett.* **93**, 255703 (2004).
19. J. Baumgartl, M. Zvyagolskaya, C. Bechinger, *Phys. Rev. Lett.* **99**, 205503 (2007).
20. D. Reinke *et al.*, *Phys. Rev. Lett.* **98**, 038301 (2007).
21. Materials and methods are available on *Science* Online.
22. J. C. Crocker, D. G. Grier, *J. Colloid Interface Sci.* **179**, 298 (1996).
23. J. C. Crocker, B. D. Hoffman, *Methods Cell Biol.* **83**, 141 (2007).
24. A. Ghosh *et al.*, *Soft Matter* **6**, 3082 (2010).
25. A. Ghosh, V. K. Chikkadi, P. Schall, J. Kurchan, D. Bonn, *Phys. Rev. Lett.* **104**, 248305 (2010).
26. P. M. Chaikin, T. C. Lubensky, *Principles of Condensed Matter Physics* (Cambridge Univ. Press, Cambridge, 2000).
27. A. Strachan, *J. Chem. Phys.* **120**, 1 (2004).
28. N. Meinshausen, P. Buhlmann, *Ann. Stat.* **34**, 1436 (2006).
29. B. B. Laird, H. R. Schober, *Phys. Rev. Lett.* **66**, 636 (1991).
30. S. N. Taraskin, S. R. Elliott, *Phys. Rev. B* **56**, 8605 (1997).
31. S. I. Simdyankin, S. N. Taraskin, M. Elenius, S. R. Elliott, M. Dzugutov, *Phys. Rev. B* **65**, 104302 (2002).

32. We acknowledge M. Widom, A. D. Dinsmore, and J. C. Crocker for valuable discussions. This work was supported by NSF through grants DMR-0645596 and DMR-0619424 (M.F.I.), the Sloan Foundation (M.F.I.), and American Chemical Society Petroleum Research Fund (M.F.I.).

Supporting Online Material

www.sciencemag.org/cgi/content/full/329/5992/656/DC1
Materials and Methods
Figs. S1 to S5
References
Movie S1

5 February 2010; accepted 29 June 2010
10.1126/science.1187988

Editor's Summary

Measuring Motion

Within a solid, atoms vibrate about their mean position in a series of frequencies known as the normal modes, which relate to the thermal and mechanical transport properties of the material. **D. Kaya *et al.*** (p. 656) used video microscopy to observe the motion of colloidal crystals made from microgel particles. The colloidal particles varied slightly in their properties, allowing the behavior of disordered materials to be probed. Long-wavelength plane-wave modes were observed, characteristic of perfect crystals, and a conventional elastic behavior, modified by short-wavelength features, was also observed, in spite of the disorder of the colloidal crystals. The analysis method will allow studies on the effects of different types of disorder on the structure of the normal modes and the elasticity in a range of material systems.